2023 IEEE/ASME International Conference on Advanced Intelligent Mechatronics (AIM)
June 28-30, 2023. Seattle, Washington, USA

Design and Control of a Stable Invertible Coaxial Actuated ROtorcraft (SICARO)

Emmanuel Tang[1], Wei Jun Ang[1], Kian Wee Tan[1] and Shaohui Foong[1]

***Abstract*— The development in the design and control of aerial actuated monowing rotorcrafts (commonly known as monocopters) has grown steadily in the past decade. To date, multiple forms of it are being produced from extensive research, however, one area that remains unexplored in this research field is the extent of how we can utilize or exploit these aerial crafts for flights. Thus, the purpose of this paper is to present and demonstrate the conception, design, and control of a new actuated monowing rotorcraft (SICARO) that is capable of rotating in different directions to fly on either side of the wing faced up in a steady and stable manner. Besides going through the research in the methodology for both the design and control of this new platform, this paper also presents results in simulation that are transferred to real experiments for comparison. To validate the effectiveness of the SICARO, the craft is flown on both sides of the wing autonomously where it holds its position in cartesian space. The RMSE for the euclidean distance in the simulations and experiments is below 1m whilst maintaining a stable body attitude.**

***Index Terms*— Single-Rotor Aerial Crafts, Monocopters, Aerial Monowing Rotorcrafts, Adaptive Control, Body Attitude Based Control, Rotational Based Control**

SUPPLEMENTARY MATERIAL:

Kindly refer to the following URL for an explicit video demonstration of the proposed design.
Video: `https://youtu.be/7y2i45iqZhw`

I. INTRODUCTION

Over the past decade, progress has been made in both the single-actuated and multi-actuated monowing rotorcraft's design and control. Numerous variations of it have been developed as a result of intensive research, but there is still much to learn about how we might use and/or exploit these aerial crafts for flight. Modern research in this particular type of aerial robot has always favored spinning in one direction (typically in line with the wing's leading edge) to achieve flight under control whilst maintaining its rotational state. The concept of flipping the monowing rotorcraft for flight is unheard of and requires the craft to rotate in the opposite direction which makes the underside of the wing the main surface that generates lift for it. For most monowing rotorcraft designs, the propeller's rotational direction to generate thrust is only fixed in one direction and the inclined change in the rate of precession generated between the angular momentum of the motor and the rotating body's torque creates an angle of attack (α) that is positive and favorable to generate lift. When flipped, thrust can still be generated from the motor as the propeller is still spinning in the same direction but this would now result in a declined change in the rate of precession between the motor's angular momentum and the body's torque. In addition, the wing may potentially have a camber that may not be effective in generating lift when flipped. Thus, most of the current designs can only cater to generating lift and flying on one side but not the other. Consequently, the goal of this work is to present and show the conception, design, and control of a revolutionary aerial craft that can rotate in different directions and fly on either side of the wing whilst maintaining attitude and positional stability.

Fig. 1: Image of the SICARO flying in the clockwise direction, the front motor stopped to prevent counter rotation

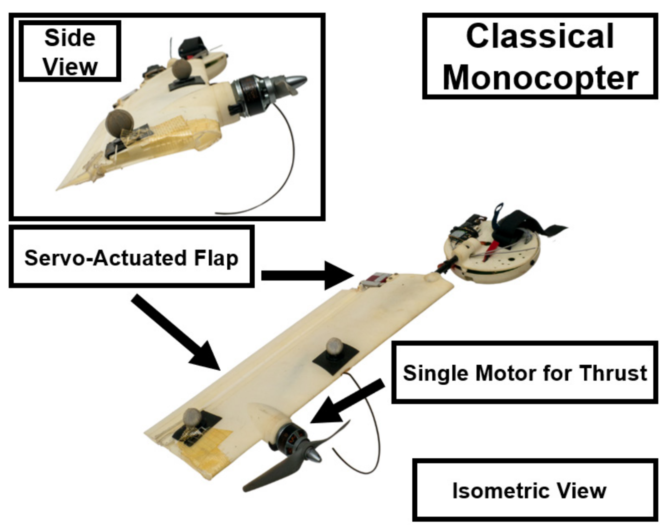

Fig. 2: Classical design of a monowing rotorcraft [9]

1 Authors are with the Engineering Product Development (EPD) Pillar of Singapore University of Technology and Design (SUTD), 8 Somapah Road, Singapore 487372 (Corresponding e-mail: foongshaohui@sutd.edu.sg)

II. Related Work

Conventional monowing rotorcraft designs may typically stick to the concept that was first introduced by [8] that uses a wing with either a conventional or symmetrical aerofoil with flaps for lift and a single actuator in the form of a motor for thrust. Research analyzing the dynamics of it in different forms further came from [6], [14], [12], and [9] who implemented the concepts in various design forms. One classic design that is consistent even with many of the variations today is shown in Fig.2. These designs, however, were only made to rotate and fly on one side which is the top side of the wing as commonly done by conventional fixed-wing aircraft. There were other designs that came in with the same wing designs but with added actuators such as [3]. Overall, these concepts were similar in the sense that none of them could rotate and fly using the underside of the wing.

III. Methodology

The methodology of this research contribution is broken down into various parts:

1) Design and dynamics of the mechanical system of SICARO
2) Implementation of an adaptive control framework for both sides of the wing (due to different actuator placements on both) and body attitude (to manage the effects of body precession during cyclic and collective control of SICARO)
3) Simulations using MATLAB Simulink in Simscape environment verify the validity and control gains of this aerial platform which are transferred to real-world experiments where the RMSE in euclidean position is measured when the SICARO attempts an autonomous position holding flight for both sides

IV. Notation

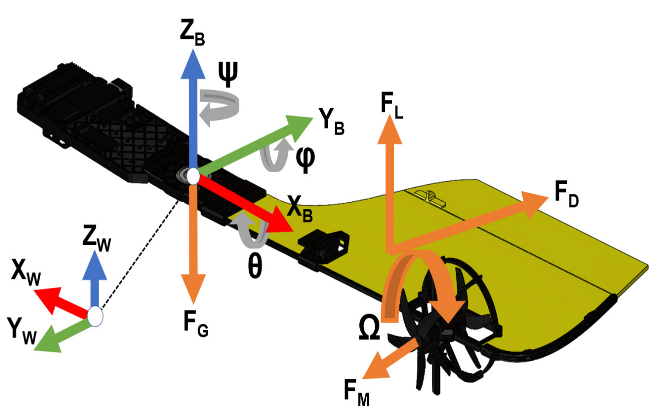

Fig. 3: Reference frames

The reference frames are labeled in Fig.3. $\{\mathbf{X_W}\ \mathbf{Y_W}\ \mathbf{Z_W}\}$ represents the orthonormal basis for the inertia frame and $\{\mathbf{X_B}\ \mathbf{Y_B}\ \mathbf{Z_B}\}$ represents the orthonormal basis for the body frame. $\mathbf{R}$ is the rotation matrix that converts coordinates in the body frame to the inertia frame and G holds the gravitational constant value of 9.81. The state vector of SICARO is written as $\mathbf{x}$ consisting of 12 dimensions:

$$\mathbf{x} = \begin{bmatrix} \rho & \eta & \upsilon & \omega \end{bmatrix} \tag{1}$$

where ρ = $[x,\ y,\ z]$ represents the position and η = $[\phi,\ \theta,\ \psi]$ represents the orientation where ϕ, θ, ψ defines the roll, pitch, and yaw in Euler angles with respect to the inertia frame. For the state derivatives, υ = $[\dot{x},\ \dot{y},\ \dot{z}]$ represents the linear velocity whilst ω = $[\dot{\phi},\ \dot{\theta},\ \dot{\psi}]$ represents angular velocity with respect to the body frame.

V. Mechanical System

A. Design

With reference to Fig.4, a flat plate wing design is chosen for its symmetry in both the top and bottom plane which allows the aircraft to have the same incident angle for lift to occur on both sides. For bi-directional flight, two counter-rotating motors were introduced to create thrust in the direction of the body's spin. Either motor is locked via braking with the Electronic Speed Controller (ESC) to prevent the rotation of the stopped motor since its rotation can cause cancellation of wing lift due to precession.

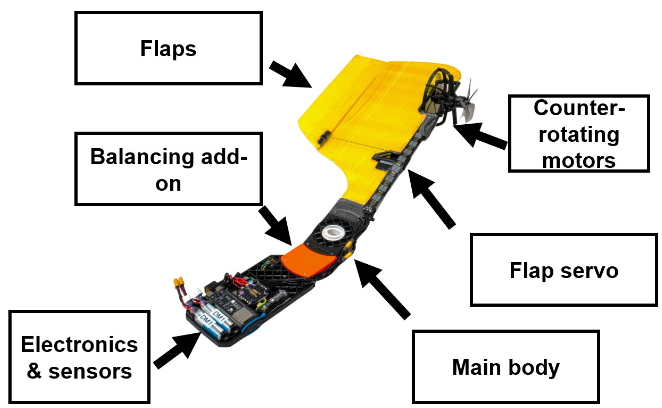

Fig. 4: SICARO hardware layout

Considerations were made in the design of the SICARO since it was based on a single motor in a single flight rotation design [13]. Additional actuators were mounted onto the airframe with minimal reduction in wing surface, which allows for minimal changes in the lift forces generated. A high-speed servo was then integrated into the chord of the wing to maintain symmetry on both wing surfaces, as well as the use of lightweight tension cables for flap actuation to minimize the variation of the center of mass of the wing. Lightweight rib structures were encouraged in the design of the airframe, allowing the load-bearing structures to maintain axial stiffness while reducing weight compared to using monolithic designs. The use of plastic pegs to join the body segments instead of traditional metal fasteners helps to further curb the weight of the airframe. To maintain about the same center of mass as the single motor and single directional design, the main body and wings were made to be modular for ease of iterations, reconfiguration, and balancing. The electronics section acts as a ballast for the actuators and wing components that are housed on the other end of the main body. The SICARO also uses an additional balancing add-on to maintain similar rotation speeds along its main wing structure compared to its predecessor with a single motor, single rotation design [8].

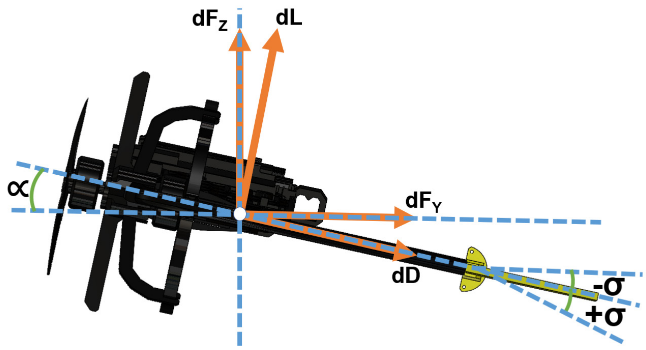

Fig. 5: SICARO side profile

In addition, the SICARO uses fully rapid prototype-able methods and materials, such as 3D printed parts and laser-cut wing surfaces. The use of off-the-shelve (OTS) components makes it flexible and fast to maintain and replace.

B. Dynamics

1) Dynamic Model: As a reference to Eqn.1, the main rigid body equations that SICARO uses were first developed by [8] and can be used to describe its 6DOF by taking in v and ω in $\mathbf{x}$.

$$\dot{\mathbf{v}} = \frac{1}{\mathbf{m}}(\sum \mathbf{F} - \omega \times (\mathbf{m}v)) \tag{2}$$

$$\dot{\omega} = \mathbf{I}^{-1}(\sum \mathbf{M} - \omega \times (\mathbf{I}\omega)) \tag{3}$$

$$\sum \mathbf{F} = \mathbf{F_G} + \mathbf{F_M} + \mathbf{F_L} + \mathbf{F_D} \tag{4}$$

$$\sum \mathbf{M} = \mathbf{M_G} + \mathbf{M_M} + \mathbf{M_L} + \mathbf{M_D} \tag{5}$$

where variables $\mathbf{m}$, $\mathbf{I}$ represent the mass and moment of inertia of SICARO. The summation of forces $\mathbf{F}$ and moments $\mathbf{M}$ in the equations themselves are a collection of them in all 3 axes and are contributed by lift, drag, gravity, and thrust from the motor respectively as in Fig.3. The motor force equation that is used to produce $\mathbf{F_M}$, can be derived from the data specification sheet from the specific motors that are used.

2) Aerodynamic Forces:

$$dL = \frac{1}{2}C_L \rho c U^2 dr \tag{6}$$

$$dD = \frac{1}{2}C_D \rho c U^2 dr \tag{7}$$

For the lift and drag equations, they were referenced from helicopter aerodynamics particularly, Blade Element Theory as thoroughly described in [7] where the lift and drag forces are accounted for each blade element across the wing surface by integrating Eqn.6 and Eqn.7 from wing root to tip. r is used to represent the width of each blade element while R represents the distance of the wing root to the tip. C_L and C_D represent the lift and drag coefficients respectively and can be obtained from the NACA aerofoil profile that the craft uses. ρ is the air density and c is the chord length of the wing. U represents the resultant inflow velocity at each blade element and can be derived by multiplying its rotation speed with its width.

$$dF_y = dL \sin\alpha - dD \cos\alpha \tag{8}$$

$$dF_z = dL \cos\alpha - dD \sin\alpha \tag{9}$$

To find out the body frame forces in $\mathbf{Z_B}$ and $\mathbf{Y_B}$ from the lift and drag respectively, Eqn.8 and Eqn.9 is used with α being the angle of attack (aka AOA) of the wing and σ being the flap angle induced to create lift. σ increases C_L when its angled down as this causes an increase in α. The ratio of σ to α varies for different aerial crafts and the ratio of α to C_L also varies depending on the aerofoil profile. A brief illustration can be seen in Fig.5 and a further in-depth derivation can be found in [5].

$$\mathbf{F_D} = -k_q \|v\| v - v k_l \tag{10}$$

$$\mathbf{M_D} = \left[-(d_l\theta + d_q\theta^2) \quad -(d_l\phi + d_q\phi^2) \quad \int_0^R \frac{r}{2} R U^2 c C_D dr \right] \tag{11}$$

Lastly, the linear and moment drag forces specifically for rotational aerial crafts like the monocopters were derived and tested in simulation to mimic reality by [10] as standard Blade Element Theory did not account for this because it was mostly generalized for helicopter aerodynamics. Variables k_q, k_l, d_l, and d_q are drag coefficients that can be adjusted to fit experimental data in the simulation.

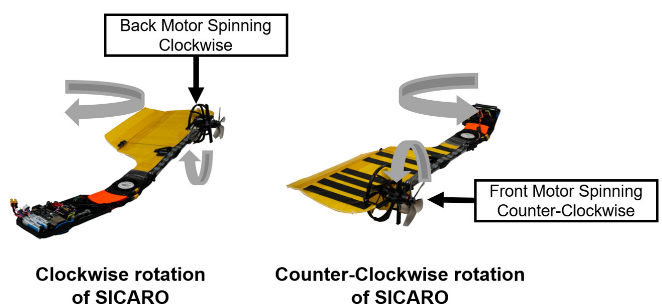

Fig. 6: Clockwise rotation for one side of the wing and counter-clockwise rotation for the other side of the wing

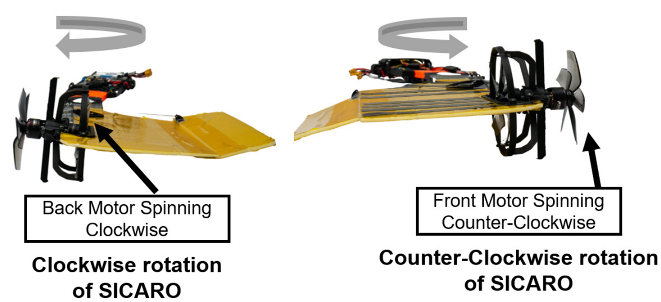

Fig. 7: Close up of the coaxial motor configuration

3) Coaxial Motor Arrangement: The SICARO can fly in the clockwise and counter-clockwise direction (when flipped) as in Fig.6 and Fig.7 by pointing its motor thrust towards the trailing edge. Both motors are spaced equally front and back from the leading edge of the wing. The thrust generated by the active motor has to spin in the correct direction to generate an angular momentum to assist the aircraft in maintaining its minimum α for the wing to generate lift - the flat plate requires a minimum incident angle of the free stream to generate lift. For the clockwise configuration (blank yellow side up), the back motor is the active motor while the front motor is inactive, with the former spinning in the clockwise direction (when viewed from the leading edge). The back motor is then stopped to prevent it from rotating in the anticlockwise direction, which can nullify the angular momentum generated from the motor system if the motor spins. Likewise, the anticlockwise configuration (black stripe side up) will have the front motor actively spinning in the anticlockwise direction, with the back motor stopped to prevent any disruption to the motor system's angular momentum.

4) Precession Required To Pitch Up: The change in precession rate generated between the motor's angular momentum and the rotating body's torque is essential to the flight of the SICARO as shown in [4]. The interaction of the rotating body's torque and the motor's angular momentum creates a resultant torque on the wing itself when in the correct orientation, creating pitching moments that aid with lift generation in Fig.8 and Fig.9 via maintaining an incident angle for the wing. In the case where both motors are active and spinning at the same rate, both motors' angular momentum would cancel each other out and that can cause the symmetrical airframe to not be able to pitch up and thus be unable to lift off. Thus, there is a minimum value required in the angular momentum of the motor system for the airframe to pitch up and lift off. The inactive motor must never be allowed to freely spin in the free stream as this will reduce the overall angular momentum of the motor system, causing a loss in pitching moment.

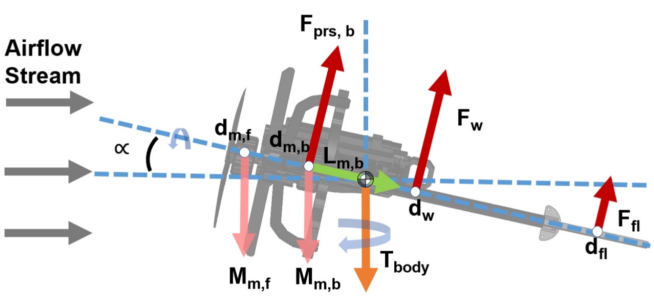

Fig. 8: Forces on the SICARO's wing profile acting about $\mathbf{X_B}$ when it rotates clockwise with the back motor

$$\mathbf{I}\dot{\omega}_x = \mathbf{F_{prs,b}}\mathbf{d_{m,b}} - (\mathbf{F_w}\mathbf{d_w} + \mathbf{F_{fl}}\mathbf{d_{fl}} + (\mathbf{M_m}\mathbf{G}(\sin\alpha)(\mathbf{d_{m,f}} + \mathbf{d_{m,b}}))) \tag{12}$$

$$\mathbf{I}\dot{\omega}_x = \mathbf{F_{prs,f}}\mathbf{d_{m,f}} - (\mathbf{F_w}\mathbf{d_w} + \mathbf{F_{fl}}\mathbf{d_{fl}} + (\mathbf{M_m}\mathbf{G}(\sin\alpha)(\mathbf{d_{m,f}} + \mathbf{d_{m,b}}))) \tag{13}$$

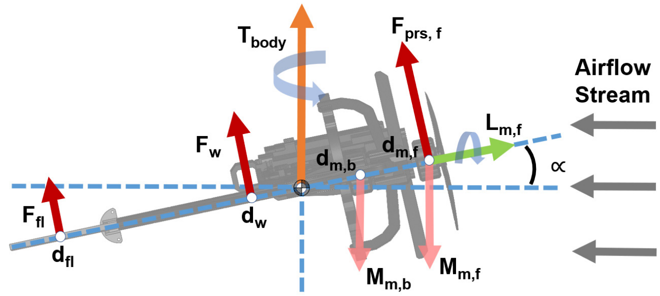

Fig. 9: Forces on the SICARO's wing profile acting about $\mathbf{X_B}$ when it rotates counter-clockwise with the front motor

Due to the placement of the motors, each motor generates a different pitching moment from the change in precession rate on the wing due to its distance relative to $\mathbf{X_B}$ in Eqn.12 and Eqn.13, where $\mathbf{M_{m,f}}, \mathbf{M_{m,b}}$ refer to the mass of the motors, $\mathbf{F_{prs,f}}, \mathbf{F_{prs,b}}$ is the force induced by the change in precession rate from each motor's angular momentum interaction with $\mathbf{T_{Body}}$, $\mathbf{F_w}, \mathbf{F_{fl}}$ are the summations forces of the wing and flap, and $\mathbf{d_w}, \mathbf{d_{fl}}, \mathbf{d_{m,f}}, \mathbf{d_{m,b}}$ refer to the relative distances from $\mathbf{X_B}$ to the forces on the wing, flaps, front motor, and back motor respectively. Eqn.12 and Eqn.13 represent the summation of moments about $\mathbf{X_B}$ when the craft is spinning clockwise and counter-clockwise respectively. This also affects how effective the flap is in manipulating the pitch of the wing due to the different magnitudes in moments about $\mathbf{X_B}$ generated by the torque that is contributed by the change in precession rate, thus requiring different gains for the flight controls in the two different configurations of flight.

VI. Adaptive Control Framework

SICARO's translation in the $\mathbf{Z}$ axis relies on collective control that primarily uses the motor's actuation whilst cyclic uses mainly the flaps for translation in the $\mathbf{X}$ and $\mathbf{Y}$ axis. This control scheme was first introduced by [8] and was referenced from helicopter aerodynamics as referred to in [7]. Gain scheduling is then introduced into this system for adaptive control for either side of the wing that is faced up and to control body attitude amplification during horizontal translation. The switching of gains is controlled and determined by sensor readings as introduced by [1] and indicated in $\mathbf{x}$.

A. Collective Control

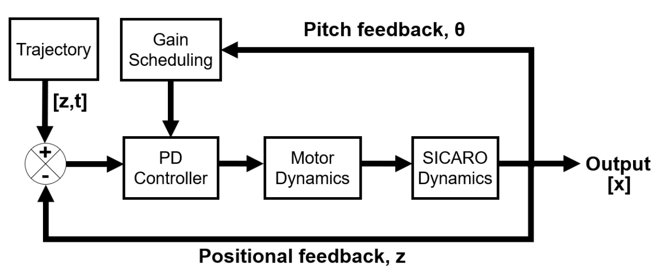

Fig. 10: Collective Control Diagram

Fig.10 refers to the control diagram for collective control. When the body's pitch θ is sensed to be greater than π or -π, this would indicate that the current underside of the wing is now the side facing up and gain scheduling would kick in to deliver a set of gains tuned for this side of the wing and vice versa. This is needed given the motor arrangements for both sides and directions as previously explained. A proportional derivative (aka PD) controller then computes the error between its current altitude and its desired height and sends the output signal to the motor where it would be coupled with pulse or step input commands to drive the motor.

B. Cyclic Control

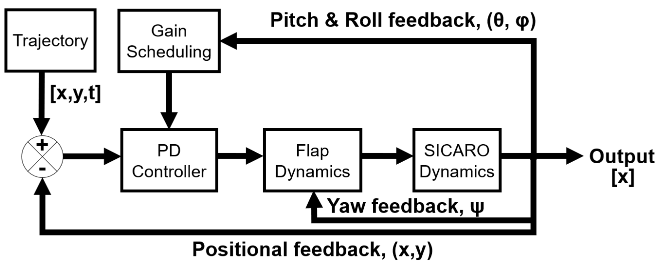

Fig. 11: Cyclic Control Diagram

Fig.11 refers to the control diagram for cyclic control. Similar to collective, when θ is sensed to be greater than π or -π, gain scheduling would issue a set of gains for the side that is facing up now for its cyclic control. The output from the PD controller designed for cyclic control would multiply with the current yaw angle ψ of the craft causing the entire tip path plane/disk to tilt in the direction of motion shown in Fig.13. ϕ is also coupled with attitude gain scheduling when it exceeds a certain absolute threshold so that the craft's overall orientation would not be overwhelmed by errant body precessions.

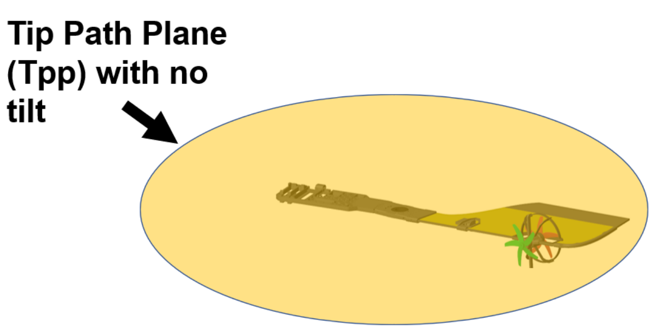

Fig. 12: Tip path plane during collective control

1) Flap dynamics for cyclic control:

$$\sigma_x = \sigma_o + (\sin(\psi + \psi_D) * (gain_x)) \tag{14}$$

$$\sigma_y = \sigma_o + (\cos(\psi + \psi_D) * (gain_y)) \tag{15}$$

The tip path plane shown in Fig.12 was observed in detail for helicopter flights as in [11] and represents the plane that connects the wing tips as SICARO rotates. This is also

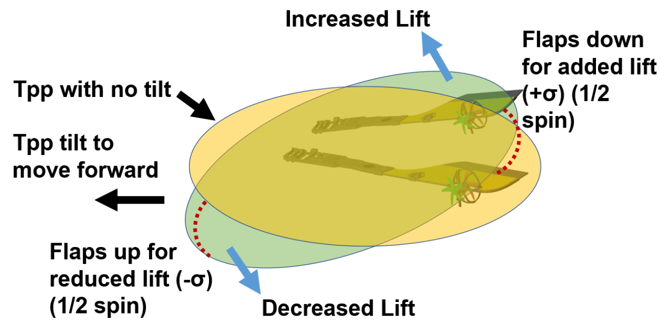

Fig. 13: Tip path plane that is tilted forward during cyclic control

referred to as the annular frame in [7] and describes the entire rotating motion of the wing as a moving disk. Assuming the ψ angle of 0 is collinear with $\mathbf{Y_W}$ and -$\frac{\pi}{2}$ for $\mathbf{X_W}$, Eqn.14 and 15 is used to send flap commands σ_x and σ_y for cyclic control where σ_o refers to the default flap angle without any α, ψ is the current craft's heading, ψ_D is the desired annular heading, and the gains are the outputs from the cyclic PD controller. Fig.13 is a simple illustration to describe this.

C. Numerical Simulation

1) Simulation Setup: The simulation is performed using MATLAB Simulink in the Simscape environment that allowed 6DOF tracking amongst many other functions. The SICARO was modeled closely to the mathematical model of the monocopter developed by [10] as well as useful empirical information provided by [9]. The SICARO was also modeled closely to the craft built in reality and is shown in Fig.14. The NACA profile 0006 matched the profile of the SICARO as it is a symmetrical airfoil and the last 2 digits were calculated based on the maximum thickness of the foil as a percentage of the wing chord as taught in [5].

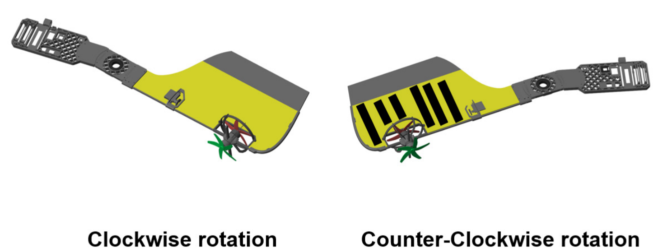

Fig. 14: The SICARO model in simulation

TABLE I: Simulation Parameters

Category	Variables
Aerodynamic Coefficients from NACA 0006	$(C_L, C_D, \frac{C_L}{C_D}, C_{L\alpha})$
Physical Properties	m = 241g
Inertial Tensor and Geometry Properties	Extracted from CAD
Environment Variables	$\rho = 1.225, G = 9.81$
Drag Coefficients	$k_q = 0.025, k_l = 0.030$ $d_l = 0.002, d_q = 0.005$

2) Simulation Results: For the PD controllers for both collective and cyclic, the Ziegler–Nichols method was implemented as referenced in [2] to the point where it is able to maintain its position steadily during hovering. The gains for both wings were different as expected due to the placement of the motors per side and after tuning, a 1.5x increase in both the proportional and derivative gains was observed for the side that had the clockwise rotation with the back motor over the side with the counter-clockwise rotation with the front motor. To control and prevent the body roll ϕ from amplifying uncontrollably, a threshold of absolute 5 degrees was set. When ϕ exceeds it, the current gains that the craft is using would be doubled in both P and D gain to force the craft to correct itself and not be consumed by errant body precessions. This continues until the craft's body roll goes below 5 degrees. The reason for choosing the body roll as the main indicator is the fact that the control of the body roll is extremely critical to the translational movement as shown in Fig.13 and under the right circumstances, it is capable of moving with minimal pitching involved. The simulation required the craft to maintain its position in both directions at a position of [0,0,2] in meters. It can be observed that the gains respectively for each side, as well as the gain scheduling for the body roll, work well in maintaining and controlling the body attitude as observed in Fig.15 and Fig.16. The body roll graph at the top has no sudden jumps or erratic motions that are often caused by errand body precessions. An example was done in simulation for both directions to not have body roll gain scheduling as shown in Fig.17 and Fig.18. The data shows erratic behavior in the body roll from the omission and both directions eventually crashed, ending the simulation prematurely. This demonstrates the importance of it for flight continuity and precession retardation. For the continued preservation of the craft in the experiment, body attitude gain scheduling remains permanent throughout.

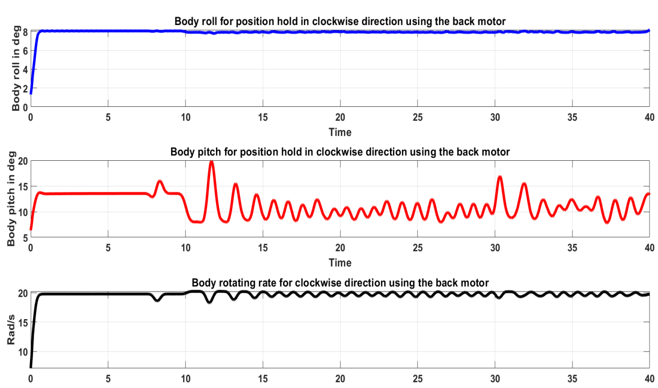

Fig. 15: Body attitude of the clockwise rotation using the back motor in simulation

The RMSE for both directional flights was recorded and shown in Table.II. The side flying clockwise with the back motor fared slightly better and with this result, these gains would now be tested in an experiment to verify the fidelity of the simulation's predicted outcome of SICARO's flight in both directions.

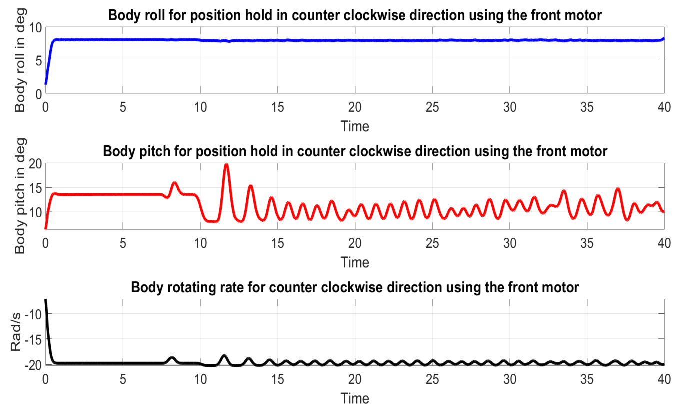

Fig. 16: Body attitude of the counter-clockwise rotation using the front motor in simulation

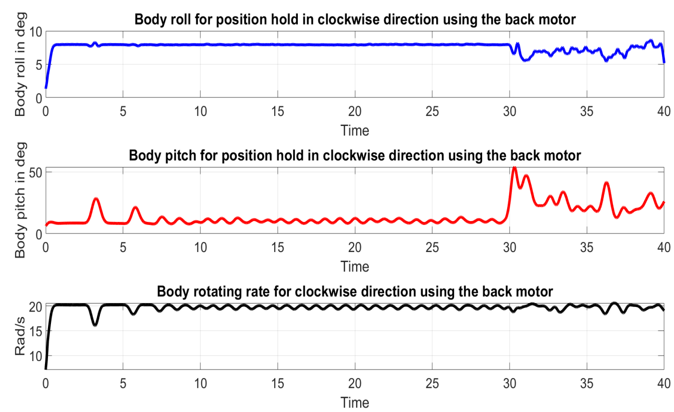

Fig. 17: Body attitude of the clockwise rotation using the back motor without body roll gain scheduling in simulation

D. Experiment

1) Experiment Setup: The experiment was conducted on the SICARO with a wingspan of 340mm using two BetaFPV 1506 3000KV motors in a coaxial setup with Gemfan 3-inch 5-blade propellers. The servo used was a Hyperion DS09 whereby the actuators are controlled by a single ESP32-S3 micro-controller unit (MCU) shown in Fig.19 that receives position feedback from an Optitrack motion capturing system. A magnetic compass, PNI3100 was used to track the heading of the aircraft while it is powered by two BetaFPV 300mah batteries in a 4S configuration through a 5VDC regulator. A radio receiver was added for human intervention as a fail-safe. For the experiment's flight objective, the SICARO will fly and hold its position autonomously at [0,0,1.5] meters in both directions.

2) Experiment Results: The gains were carried from the simulation into the experiment. Although the simulation model is modeled closely to the real craft, the real world possesses a lot more factors that can never be fully accounted for. The magnitude of gains in the simulation was relatively large for the real craft and had to be scaled down by at least

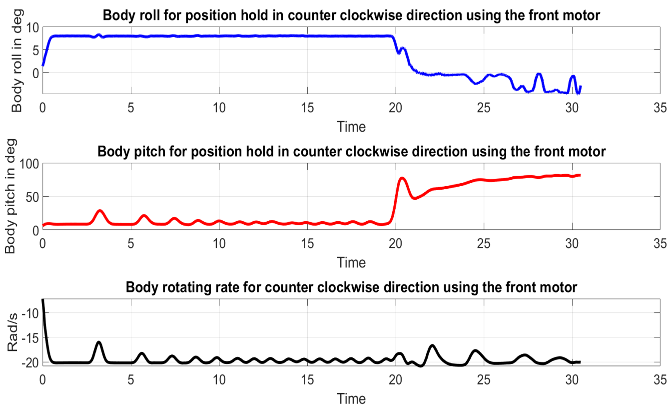

Fig. 18: Body attitude of the counter-clockwise rotation using the front motor without body roll gain scheduling in simulation

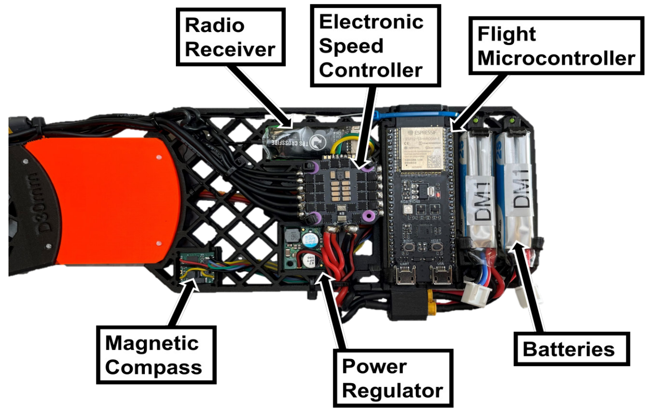

Fig. 19: Components on the Electronics ballast

TABLE II: Simulation RMSE in Euclidean Position

Wing side	Error(m)
Front Motor (CCW)	0.041
Back Motor (CW)	0.037

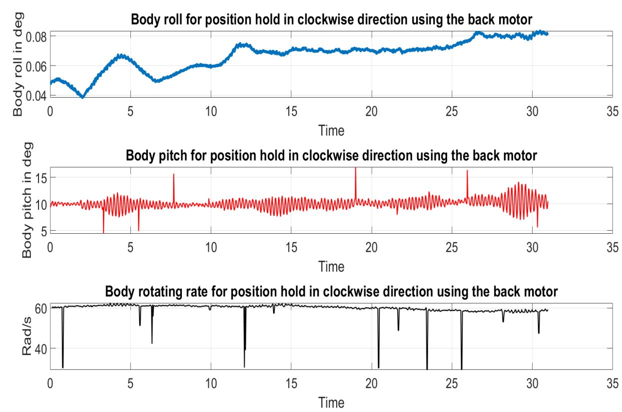

Fig. 20: Body attitude of the clockwise rotating flight using the back motor in experiment

half due to the sensitivity and noise in the electronics and actuation. This, however, did not change the ratio between the gains in the clockwise and counter-clockwise directions with the ratio of 1.5:1 still standing. The gain scheduling for body roll was also preserved at twice the gains should it exceed an absolute of 5 degrees.

TABLE III: Experiment and Simulation RMSE in Euclidean Position

Wing side	Simulation Error(m)	Experiment Error(m)
Front Motor (CCW)	0.041	0.836
Back Motor (CW)	0.037	0.809

E. Discussion

With reference to Table.III, although the RMSE values are individually different, the results are the same between simulation and experiments with the wing side that is rotating clockwise with the back motor outperforming the side that is going counter-clockwise with the front motor. The graphs in Fig.20 and Fig.21 also show steady and non-erratic responses in the body roll like Fig.15 and Fig.16 which reaffirms the need for the gain scheduling in the body roll to aid in retarding and minimizing excessive body roll amplifications due to errant body precessions. Regarding the comparisons in RMSE between both sides, the collective actuation from the front motor induces a larger pitching moment due to precession which causes the body to precess in position compared to the back motor. This makes it harder to correct the flap cyclic actuation. As a result, the front motor spinning counter-clockwise does not perform as well compared to the back motor spinning clockwise due to the collective motor actuation. The larger pitching angles seen by the counter-clockwise configuration when cyclic actuation is applied can cause a significant drop in ω_z[1] about $\mathbf{Z_B}$ due to the angular momentum being converted to lift when the wing experiences a high α. ω_z immediately returns to the average rotation rate when the flap returns to the neutral position.

Lastly, due to the high rotation rates of the airframe (up to 12hz) and limited capturing refresh rates, tracking data from the motion capture system can be noisy due to bad tracking or complete loss of tracking during the flights. This is a huge factor that contributes to the tracking noise during the experiment. In addition, environmental factors within the tracking area such as random drafts, magnetic interference, and ambient lighting are causes for discrepancies in the controls and results compared to the simulations. Furthermore, as the batteries drain during flight, the battery voltage affects how reactive the collective and cyclic actuation is due to the lower actuation forces of both motors and servo with the lower voltages.

F. Conclusion

The SICARO is able to perform reasonably with the ratio of gains from the simulation, and the simulations have shown that the performance of the craft flying in a clockwise direction with the back motor is better than the side flying

[1]Only absolute values were plotted for ω_z during both experiments

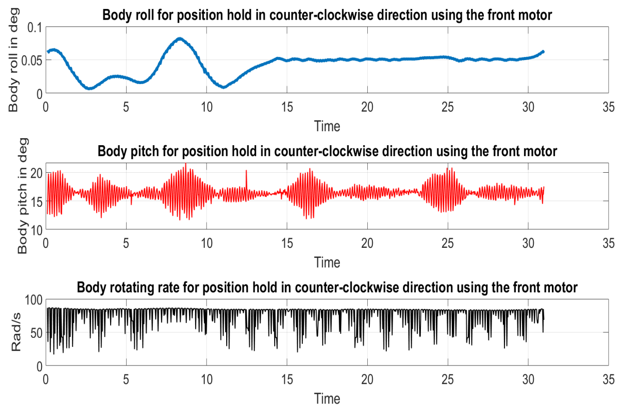

Fig. 21: Body attitude of the counter-clockwise rotating flight using the front motor in experiment

Fig. 22: Clockwise rotating flight using the back motor in experiment

in a counter-clockwise direction with the front motor, which is coherent with the experiment results where the RSME of the clockwise configuration yielded a lower value.

G. Future Work

A reduction in the number of motors used can help with the differences in pitching moment due to the precession of the body since the source of the torque will be in the same position, allowing for identical gains on the flight regimes. The lighter aircraft will also allow for better flight efficiency and a different control method which may provide better control in the acceleration of the aircraft. This could possibly help with the inherent position precession of the aircraft.

H. Acknowledgements

The authors thank Mr. James Kusuma Dewa Halim for his contribution to the software stacks used in the experiments.

References

[1] Yann Ameho, Fabien Niel, François Defaÿ, Jean-Marc Biannic, and Caroline Bérard. Adaptive control for quadrotors. In *2013 IEEE International Conference on Robotics and Automation*, pages 5396–5401, 2013.

Fig. 23: Counter-clockwise rotating flight using the front motor in experiment

[2] Karl Johan Åström and Tore Hägglund. Revisiting the ziegler–nichols step response method for pid control. *Journal of process control*, 14(6):635–650, 2004.

[3] Hitesh Bhardwaj, Shane Kyi Hla Win, Luke Soe Thura Win, Danial Sufiyan, and Foong Shaohui. P.i.d. based sliding mode control of asynchronous multi-actuator monocopter. In *2021 IEEE/ASME International Conference on Advanced Intelligent Mechatronics (AIM)*, pages 239–246, 2021.

[4] Xinyu Cai, Shane Kyi Hla Win, Luke Soe Thura Win, Danial Sufiyan, and Shaohui Foong. Cooperative modular single actuator monocopters capable of controlled passive separation. In *2022 International Conference on Robotics and Automation (ICRA)*, pages 1989–1995. IEEE, 2022.

[5] Snorri Gudmundsson. *General aviation aircraft design: Applied Methods and Procedures*. Butterworth-Heinemann, 2013.

[6] James Houghton and Woody Hoburg. Fly-by-wire control of a monocopter. *Massachusetts Institute of Technology, Project Report*, 2008.

[7] Stewart Houston. Principles of helicopter aerodynamics. jg leishman. cambridge university press, the edinburgh building, cambridge cb2 2ru, uk. 2000. 496pp. illustrated.£ 60 isbn 0-521-66060-2. *The Aeronautical Journal*, 104(1038):390–390, 2000.

[8] Andreas Kellas. *The guided samara: design and development of a controllable single-bladed autorotating vehicle*. PhD thesis, Massachusetts Institute of Technology, 2007.

[9] Jun En Low, Ying Hong Pheh, and Shaohui Foong. Analysis of wing twist effects on hover flight dynamics of a single rotor aerial craft. In *2016 IEEE International Conference on Advanced Intelligent Mechatronics (AIM)*, pages 323–328, 2016.

[10] Gašper Matič, Marko Topič, and Marko Jankovec. Mathematical model of a monocopter based on unsteady blade-element momentum theory. *Journal of Aircraft*, 52(6):1905–1913, 2015.

[11] Lorenzo Trainelli, CARLO RIBOLDI, Mattia Bucari, et al. Observing the angle of attack of the tip-path plane from rotor blade measurements. In *41st European Rotorcraft Forum*, pages 1190–1201. Curran Associates, 2015.

[12] Evan R Ulrich, Imraan Faruque, Jared Grauer, Darryll J Pines, J Sean Humbert, and James E Hubbard Jr. Control model for robotic samara: Dynamics about a coordinated helical turn. *Journal of guidance, control, and dynamics*, 33(6):1921–1927, 2010.

[13] Luke Soe Thura Win, Shane Kyi Hla Win, Danial Sufiyan, Gim Song Soh, and Shaohui Foong. Achieving efficient controlled flight with a single actuator. In *2020 IEEE/ASME International Conference on Advanced Intelligent Mechatronics (AIM)*, pages 1625–1631. IEEE, 2020.

[14] Harold Youngren, Steve Jameson, and Brian Satterfield. Design of the samarai monowing rotorcraft nano air vehicle. In *Proceedings of the American Helicopter Society AHS 65th Annual Forum and Technology Display*, 2009.